Applied Physics Letters ARTICLE scitation.org/journal/apl

Stretching ReS_2 along different crystal directions: Anisotropic tuning of the vibrational and optical responses

Cite as: Appl. Phys. Lett. **120**, 063101 (2022); doi: 10.1063/5.0081127
Submitted: 7 December 2021 · Accepted: 19 January 2022 ·
Published Online: 7 February 2022

View Online Export Citation CrossMark

Hao Li,[1] Der-Yuh Lin,[2] Anna Di Renzo,[1,3] Sergio Puebla,[1] Riccardo Frisenda,[1] Xuetao Gan,[4] Jorge Quereda,[5] Yong Xie,[1,6] Abdullah M. Al-Enizi,[7] Ayman Nafady,[7] and Andres Castellanos-Gomez[1,a)]

AFFILIATIONS

[1]Materials Science Factory, Instituto de Ciencia de Materiales de Madrid (ICMM-CSIC), Madrid E-28049, Spain
[2]National Changhua University of Education, Bao-Shan Campus, No. 2, Shi-Da Rd., Changhua City 500, Taiwan
[3]Dipartimento di Matematica e Fisica "E. De Giorgi," Campus Ecotekne, Università del Salento, Via Arnesano, 73100 Lecce, Italy
[4]Key Laboratory of Light Field Manipulation and Information Acquisition, Ministry of Industry and Information Technology, and Shaanxi Key Laboratory of Optical Information Technology, School of Physical Science and Technology, Northwestern Polytechnical University, 710129 Xi'an, China
[5]Nanotechnology Group, USAL–Nanolab, Univesidad de Salamanca, Salamanca, Junta de Castilla y León 37007, Spain
[6]Key Laboratory of Wide Band-Gap Semiconductor Technology, School of Advanced Materials and Nanotechnology, Xidian University, Xi'an 710071, China
[7]Department of Chemistry, College of Science, King Saud University, Riyadh 11451, Saudi Arabia

Note: This paper is part of the APL Special Collection on One-Dimensional van der Waals Materials.
[a)]**Author to whom correspondence should be addressed:** andres.castellanos@csic.es

ABSTRACT

Rhenium disulfide (ReS_2) is a semiconducting two-dimensional material with marked in-plane structural anisotropy. This lattice anisotropy is the stem of many quasi-1D properties observed in this material. In this work, we focus on strain engineering of optical and vibrational properties through mechanical deformations of the lattice. In particular, the exciton energy can be shifted by applying uniaxial strain, and the gauge factor is six times more pronounced when the strain is applied along the *b*-axis than in perpendicular to the *b*-axis of the ReS_2 lattice. Moreover, we also observed how the two most prominent Raman modes can be shifted by uniaxial strain, and the shift strongly depends on the alignment between the uniaxial strain direction and the *a*- and *b*-axes of the ReS_2 lattice.

Strain engineering provides a powerful route to tune electrical, optical, thermal, and mechanical properties of two-dimensional (2D) materials at will.[1–16] In fact, this family of materials is very resilient to mechanical deformations, and they can sustain strains up to 20% without breaking, fully recovering when the strain is released.[17–19] Moreover, the applied strain can be effectively adjusted by simply placing a 2D material onto a flexible substrate and bending it in a controlled way.[20,21] This method allows one to continuously tune the properties of 2D materials.

Interestingly, for the 2D materials with strong in-plane anisotropy, uniaxial strain can have a different effect when applied along different crystal orientations.[22–30] This provides an extra degree-of-freedom to tune the properties of 2D materials through strain engineering. To date, however, only a few experimental works have exploited this new degree-of-freedom.[24,31–35] ReS_2, as a 2D group VII transition metal dichalcogenide, possesses a characteristic anisotropic structure compared to molybdenum and tungsten dichalcogenides, which contributes to anisotropic in-plane optical, vibrational, and other properties.[36–42] Although these anisotropic optical and vibrational properties of layered ReS_2 crystals have been previously well probed, strain engineering based on the anisotropy remains unexplored. Here, we study the effect of uniaxial strain, applied along

different crystal orientations on the vibrational and optical properties of the exfoliated ReS_2 flakes. By testing the differential reflectance test of layered ReS_2 under strain along the two main crystalline orientations, a clear redshift on the excitonic peak could be observed, and the redshift rate of the exciton reaches a maximum and a minimum when uniaxial strain is applied along the directions that are parallel and perpendicular to the *b*-axis of ReS_2, respectively. Furthermore, Raman spectroscopy is carried out to study vibrational anisotropy under strain along different directions, from which it is shown that the gauge factor of Raman redshift for the different vibrational modes reaches a maximum with uniaxial strain applied along the specific crystalline orientations corresponding to these vibrational Raman modes. The results presented here provide the first step to use optical spectroscopy techniques to determine the in-plane strain profiles in ReS_2 flakes and demonstrate the possibility to tune the anisotropic properties of ReS_2 through uniaxial strain applied along different crystal axes.

ReS_2 flakes were prepared by mechanical exfoliation of bulk crystals both in-house grown (further described in the supplementary material—Materials and Method section and Fig. S1) and commercially available (HQ Graphene) with Nitto SPV 224 tape. The cleaved ReS_2 are then transferred onto a gel-film (WF ×4 6.0 mil, by Gel-Pak) substrate by adhering it to the Nitto tape surface and peeling it off gently. Next, suitable ReS_2 flakes are identified by transmission-mode optical microscopy and transferred onto the center of a disk-shaped polycarbonate substrate by an all-dry deterministic transfer method.[43–45] This disk-shaped flexible substrate can be mounted into a custom-built three-point bending apparatus to apply strains along different in-plane directions as described in detail in our previous work (see also the supplementary material—Materials and Method section and Fig. S2).[31]

Figure 1(a) shows an optical micrograph of a ReS_2 flake (~7 nm thick, see Fig. S3 in the supplementary material) transferred onto the center of a polycarbonate disk-shaped substrate. Several techniques can be used to find the crystal orientation of the exfoliated flakes. Among these techniques, differential reflectance[49] provides a convenient and nondestructive way of determining the crystalline orientations. Figure 1(b) shows a collection of differential reflectance spectra acquired when illuminating the sample with linearly polarized light along different directions. In our experiment, the angle between the linear polarization axis and the horizontal axis is labeled as θ. It has been reported that ReS_2 differential reflectance spectra present a strong peak feature attributed to the generation of excitons, whose intensity depends on the alignment between the incident linearly polarized light and the crystal directions of the ReS_2 flake.[40] When the light is linearly polarized parallel to the *b*-axis of the ReS_2 lattice, the intensity of this excitonic peak reaches a minimum value (see the supplementary material of Ref. 40). Figure 1(c) shows a polar plot summarizing the relationship between the angle θ and the intensity of the excitonic peak feature. The polar plot shows how the minimum intensity is reached when the light is polarized almost parallel to the horizontal axis, indicating that the *b*-axis of the crystal is also oriented along this direction.

We have also used polarized Raman spectroscopy as a complementary approach to determine the crystal axes of ReS_2 flakes. For this experiment, the excitation laser is kept fixed [polarized along the vertical axis in the microscope image of Fig. 2(a)], and the ReS_2 sample is being rotated. The angle between the flake edge highlighted with the dashed blue line and the excitation polarization axis is labeled now as θ. Figure 2(a) shows an example of a ReS_2 flake (~1–2 layers thick according to its reflectance spectra,[40] see Fig. S4 in the supplementary material) whose crystal orientation is characterized through polarized Raman spectroscopy. Figure 2(b) shows a collection of Raman spectra collected for different θ values. The spectra present two prominent Raman peaks,[36,46] labeled as Raman modes III (A_g1) and V (A_g7) according to Refs. 31 and 47. The intensity of these two Raman peaks

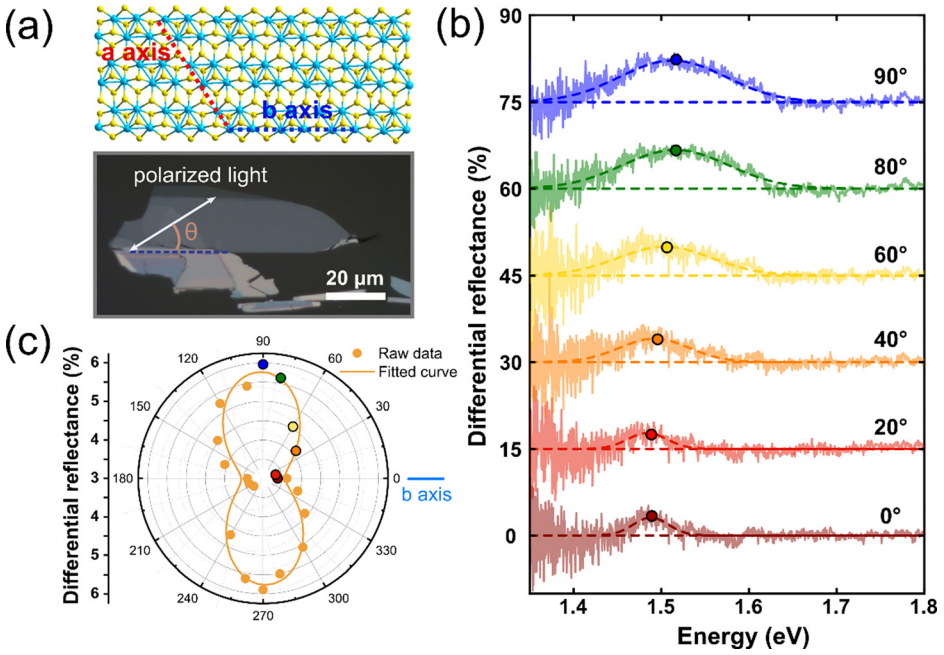

FIG. 1. The identification of the crystalline orientation of a ReS_2 flake by differential reflectance measurements. (a, top) 3D representation of the crystal structure of ReS_2 where the in-plane anisotropy and crystalline orientations can be clearly identified (blue atom: Re, yellow atom: S). (a, bottom) Optical micrograph of a layered ReS_2 flake. In the polarization-dependent reflectance measurements, θ is defined as the angle between the cleaved long straight edge of the flake and polarized light. (b) Micro-reflectance spectra of the ReS_2 flake (unintentionally strained during fabrication) as a function of the polarized light rotation (counterclockwise direction) angle from 0° to 90° (the cleaved edge is parallel to the horizontal axis corresponding to 0°). The spectra have been vertically offset by 15% to facilitate the comparison. (c) Polar plot of the differential reflectance intensity at ~1.5 eV for different angles between the incident linearly polarized light and the cleaved edge of the ReS_2 flake. The specially colored circles correspond to the spectra shown in (b).

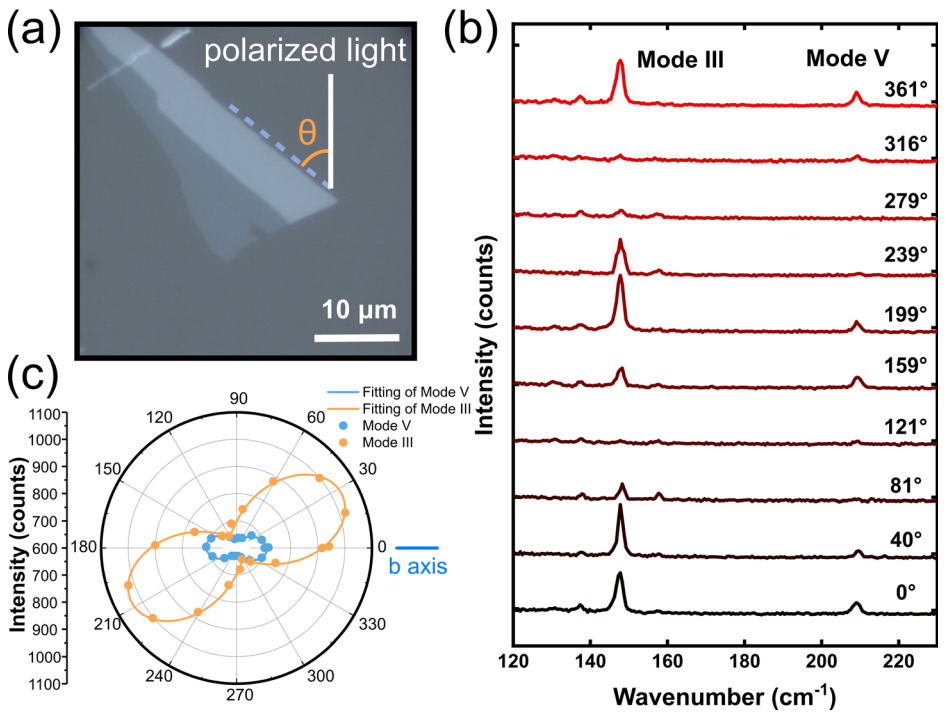

FIG. 2. The identification of the crystalline orientation of the ReS_2 sample by Raman spectroscopy. (a) The optical microscopy image of the ReS_2 flake. In the polarization-dependent Raman measurements, θ is defined as the angle between the cleaved long straight edge of the flake and polarized light. (b) Raman spectra of the ReS_2 flake (unstrained) as a function of the sample rotation (counterclockwise direction) angle from 0° to 361° while incident light is linearly polarized parallel to the vertical axis. The spectra have been vertically offset by 400 counts to facilitate the comparison. (c) Polar plot of the Raman intensity under mode III and mode V for different angles between the polarized light and the cleaved edge of the ReS_2 flake.

strongly depends on the angle θ. In fact, it has been reported how the intensity of mode V reaches a maximum intensity, when the excitation polarization is parallel to the *b*-axis of the ReS_2 flake.[31] Mode III, on the other hand, becomes maximum when the *b*-axis and the linear polarization form an angle of 30°.[39] Figure 2(c) shows a polar plot with the intensity of the mode III and mode V Raman peaks as a function of the angle θ. This plot confirms that the *b*-axis of the ReS_2 flake is parallel to the crystal edge highlighted with the dashed blue line in Fig. 2(a).

In the following, we will study the effect of uniaxial strain, applied along different crystal orientations, on the differential reflectance spectra of ReS_2. As described above, the ReS_2 flake under study was transferred on the center of a disk-shaped polycarbonate substrate that can be mounted in a three-point bending apparatus to apply uniaxial strain by controllably bending the disk. By rotating the disk-shaped substrate between different straining cycles, one can apply the uniaxial strain to ReS_2 along different crystal orientations. All along these strain engineering experiments, the incident light is linearly polarized perpendicular to the *b*-axis of the crystal to optimize the intensity of the observed excitonic feature in the differential reflectance spectra. Then, several differential reflectance spectra are acquired as a function of the angle between the straining direction (horizontal axis) and the *b*-axis of the crystal (previously determined by linearly polarized differential reflectance and Raman spectroscopies). Figure 3(a) shows an optical micrograph of a ReS_2 flake with the straining direction almost parallel to the *b*-axis of the crystal (with an angle of −1°) and the differential reflectance spectra collected as a function of the uniaxial strain applied. The excitonic peak, which at zero strain is centered around at ∼1.55 eV, shifts toward lower energies upon increasing tensile uniaxial strain. Interestingly, when the sample is rotated and the strain is applied perpendicular to the *b*-axis of the crystal [Fig. 3(b)], the excitonic peak shifted as small as ∼−4 meV upon 0.39% straining. Figure 3(c) shows the extracted exciton energies as a function of the applied uniaxial strain for some selected alignments between the straining direction and the *b*-axis of the flake. One can see how the exciton energy shift rate depends on the crystal direction along different straining directions. From the slope of these datasets, one can extract the gauge factor, i.e., the exciton energy shift per percentage of uniaxial tension. For a configuration where the strain is applied almost parallel to the b-axis of the crystal, the gauge factor is ∼−60 meV/% while it drops to ∼−10 meV/% when the strain is applied perpendicular to the *b*-axis. Figure 3(d) summarizes all the extracted gauge factors for different angles between the straining direction and the *b*-axis. The experimental dataset can be fitted to a cosine function with the maximum at 0°, 180°, and 360° of ∼−70 meV/% and the minimum at 90° and 270° of ∼−15 meV/%. This experimentally observed anisotropic strain tuning of the exciton peaks can be understood in terms of the band structure changes undertaken by ReS_2 when uniaxial strain is applied along different crystal directions. Yu *et al.* predicted, through density functional calculations, a bandgap reduction (that would translate into a exciton energy reduction) of −60 meV/% for strains along the *b*-axis and of −30 meV/% for strain along the *a*-axis,[48] in reasonable agreement with our experimental observation.

The anisotropy ratio of the gauge factor can be defined as

$$\text{Anisotropy ratio} = (GF_{max} - GF_{min})/(GF_{max} + GF_{min}) \cdot 100\%,$$

where GF_{min} and GF_{max} stand for the minimum and maximum gauge factors, respectively. This magnitude will be 0% for perfectly isotropic materials. From the cosine-function fit of Fig. 3(d), we can estimate an

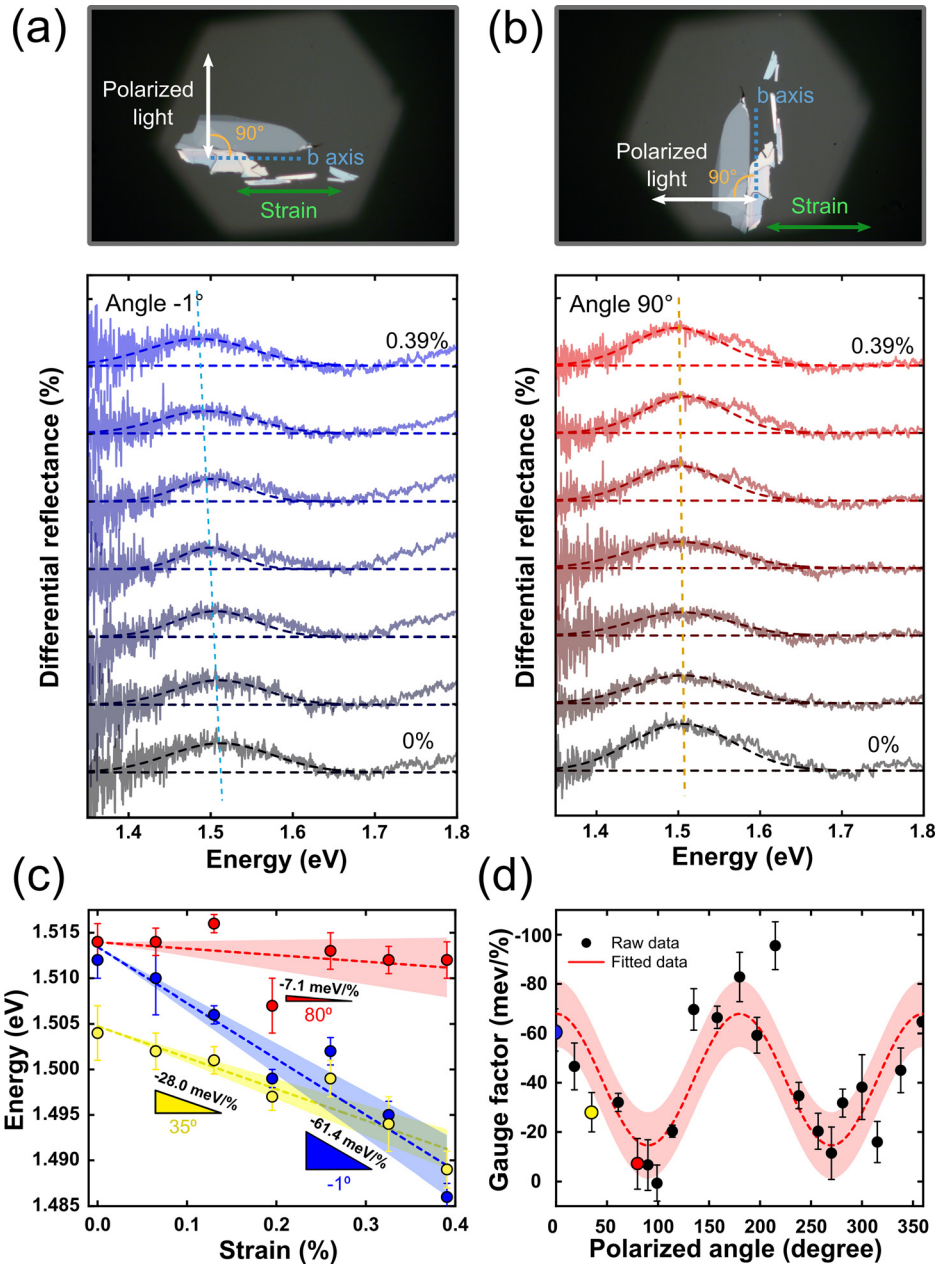

FIG. 3. Angle-resolved micro-reflectance spectra of ReS_2 under different uniaxial strain from 0% to 0.39%. (a) and (b) Micro-reflectance spectra collected when the uniaxial strain direction is parallel and perpendicular to the *b*-axis of the ReS_2 flake, respectively. (c) Exitonic peak energy as a function of the applied uniaxial strain under different orientation angles (−1°, 35°, and 80°). A linear fit is used to extract the gauge factor. The shaded area around the dashed lines represents the uncertainty of the gauge factor extracted from the linear fit. (d) Angular dependence of the ReS_2 exciton gauge factor as a function of the sample rotation angle. A fit to a cosine function is used to study the dependence between the polarized angle and the exciton gauge factor. Red shaded area around the dashed fit indicates the uncertainty of the cosine function fit. All the tests are carried out with the flake *b*-axis direction perpendicular to the incident linearly polarized light for obtaining the maximum peak intensity. Then the strain direction is kept fixed while the sample and polarization are rotated simultaneously in a counterclockwise direction to keep the polarized incident light and the *b*-axis perpendicular along the whole experiment.

anisotropy ratio of ∼80%, much larger than the reported value for black phosphorus, another 2D material with a remarkable in-plane structural anisotropy that reached ∼3%.[33] This value is even comparable with the anisotropy ratios recently found in $ZrSe_3$, the material with the largest anisotropy measured so far, which ranges between ∼73% and 100%.

We have also studied the effect of uniaxial strain, applied along different crystal directions, on the Raman modes of ReS_2. The measurement is carried out with the excitation laser linearly polarized perpendicularly to the direction of uniaxial strain. By rotating the disk-shaped substrate, we can apply the strain along different crystal directions in the sample. The sample starts with its *b*-axis parallel to the strain direction (defined as 0°), and it is subjected to a uniaxial straining cycle. Figure 4(a) shows Raman spectra upon different uniaxial strains up to 0.65%. The spectra have been zoomed-in around mode V to facilitate tracking the subtle strain-induced shift of the Raman mode. After the strain cycle is completed, the sample is rotated by ∼20° to perform another straining cycle. Figure 4(b) shows an example of another straining test carried out when the sample has its *b*-axis forming ∼80° with

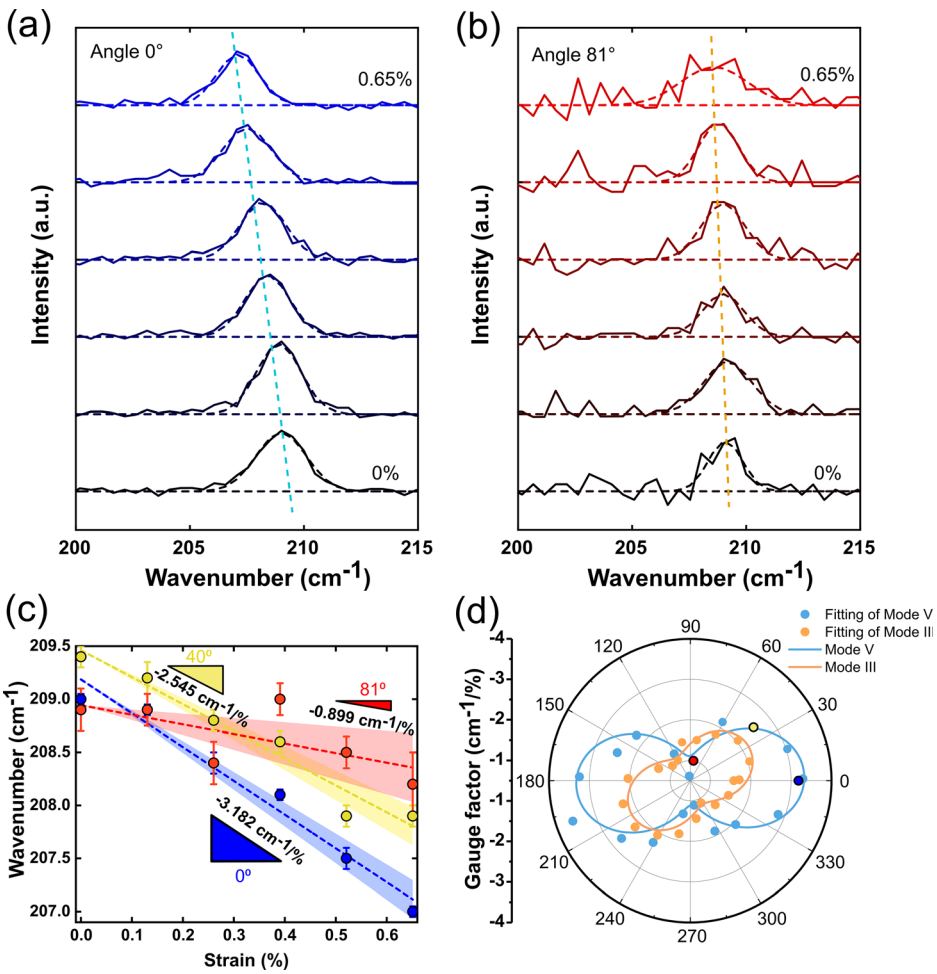

FIG. 4. Angle-resolved Raman spectra of ReS_2 at mode V under different uniaxial strain from 0% to 0.65%. (a) and (b) Raman spectra collected when the uniaxial strain direction is parallel and nearly perpendicular to the *b*-axis of the ReS_2 flake, respectively. (c) Raman shift at mode V as a function of the applied uniaxial strain under different orientation angles (0°, 40°, and 81°). A linear fit is used to extract the gauge factor. The shaded area around the dashed lines represents the uncertainty of the gauge factor extracted from the linear fit. (d) Angular dependence of the ReS_2 Raman shift gauge factor as a function of the sample rotation angle in polar coordinates. All the tests are carried out with the straining direction parallel to the horizontal axis and the laser polarized parallel to the vertical axis. Then the strain direction and the polarized laser light are kept fixed while the sample is rotated in the counterclockwise direction during the experiment to collect the Raman spectra.

the straining axis. For this configuration, uniaxial strain has a negligible effect on the position of Raman mode V, indicating the anisotropic effect of uniaxial strain in strain-tuning of the vibrational properties of ReS_2.

Figure 4(c) shows a summary of Raman peak positions vs uniaxial strain for datasets collected when the strain is applied along different crystal directions (0° is parallel to the *b*-axis; 120° is parallel to the *a*-axis). Linear fits have been used to extract the Raman gauge factors and the Raman peak shift in cm^{-1} per % of uniaxial strain.

For simplicity, we have focused the discussion above to Raman mode V. Similar results for Raman mode III are depicted in supplementary material, Fig. S5.

The resulting gauge factors for different crystal orientations are shown in Fig. 4(d). There the anisotropic character of the strain tunability is evident: For mode V, the strain-induced redshift becomes maximal when the strain is applied parallel to the *b* axis, reaching a gauge factor of around $-3.18\,cm^{-1}/\%$. A minimum gauge factor of around $-0.90\,cm^{-1}/\%$ is obtained when the strain is applied parallel and perpendicular to the *b* axis. For mode III, the gauge factor maximizes for strain applied at an angle of 30° relative to the *b*-axis, reaching a value of around $-2.04\,cm^{-1}/\%$. For strain perpendicular to this direction, the gauge factor decreases to $-1.09\,cm^{-1}/\%$.

It is worth noting that, according to recent literature works for polarization-resolved Raman spectroscopy of ReS_2, Raman vibrational modes III and V reach a maximal coupling with the electric field of light for polarization oriented at 30° and 0°, respectively, relative to the *b* crystalline axis. These angles of polarization accurately match the directions of strain for which we obtain maximal strain gauge factors.

In summary, we subjected thin ReS_2 flakes to uniaxial tensile strain applied along different crystal directions and studied the effect of this strain on their optical and vibrational properties. We observed how the exciton peak, present in the differential reflectance spectra, redshifts at a different rate when strain is applied along different directions. When the strain is parallel to the *b*-axis of the crystal, it reaches the maximum strain tunability (∼−60 meV/%), and it reaches a minimum when the strain is applied perpendicular to the *b*-axis (∼−10 meV/%). Regarding the vibrational properties, we found that two Raman modes (mode III and mode V) are the most sensitive to strain. We also observed a shift of these Raman peaks upon straining, but now each mode responds differently to strains along different directions. Mode V reaches a maximum shift rate when the strain is

applied parallel to the *b*-axis ($\sim -3.3\,cm^{-1}/\%$) and a minimum for strain perpendicular to the *b*-axis ($\sim -1\,cm^{-1}/\%$). Mode III, on the other hand, presents a different symmetry: it reaches a maximum strain tunability for tension parallel to an axis forming 30° with the *b*-axis ($\sim -2\,cm^{-1}/\%$) and a minimum value for strain perpendicular to that axis ($\sim -1\,cm^{-1}/\%$). This work provides a better understanding of the role of strain on the properties of two-dimensional materials with strong in-plane anisotropy.

See the supplementary material for materials and methods, atomic force microscopy characterization of the ReS_2 flake measured for reflectance tests in the main text, differential reflectance of the ReS_2 flake measured for Raman spectroscopy tests in the main test, angle-resolved Raman spectra of ReS_2 at mode III under different uniaxial strains from 0% to 0.65%, and growth of ReS_2 crystals.

This project was funded by the European Research Council (ERC) under the European Union's Horizon 2020 research and innovation program (Grant Agreement No. 755655, ERC-StG 2017 project 2D-TOPSENSE). H.L. acknowledges Grant No. 201907040070 from the China Scholarship Council (CSC). The authors extend their sincere appreciation to the Distinguished Scientist Fellowship Program (DSFP) at King Saud University for funding this work.

AUTHOR DECLARATIONS

Conflict of Interest

The authors declare no conflict of interest.

DATA AVAILABILITY

The data that support the findings of this study are available from the corresponding author upon reasonable request.

REFERENCES

[1]R. Roldán, A. Castellanos-Gomez, E. Cappelluti, and F. Guinea, J. Phys. Condens. Matter **27**, 313201 (2015).
[2]B. Amorim, A. Cortijo, F. de Juan, A. G. Grushin, F. Guinea, A. Gutiérrez-Rubio, H. Ochoa, V. Parente, R. Roldán, P. San-Jose, J. Schiefele, M. Sturla, and M. A. H. Vozmediano, Phys. Rep. **617**, 1 (2016).
[3]A. Chaves, J. G. Azadani, H. Alsalman, D. R. da Costa, R. Frisenda, A. J. Chaves, S. H. Song, Y. D. Kim, D. He, J. Zhou, A. Castellanos-Gomez, F. M. Peeters, Z. Liu, C. L. Hinkle, S.-H. Oh, P. D. Ye, S. J. Koester, Y. H. Lee, P. Avouris, X. Wang, and T. Low, npj 2D Mater. Appl. **4**, 29 (2020).
[4]L. Du, T. Hasan, A. Castellanos-Gomez, G.-B. Liu, Y. Yao, C. N. Lau, and Z. Sun, Nat. Rev. Phys. **3**, 193 (2021).
[5]S. Yang, Y. Chen, and C. Jiang, InfoMat **3**, 397 (2021).
[6]J. Du, H. Yu, B. Liu, M. Hong, Q. Liao, Z. Zhang, and Y. Zhang, Small Methods **5**, 2000919 (2021).
[7]Y. Han, J. Zhou, H. Wang, L. Gao, S. Feng, K. Cao, Z. Xu, and Y. Lu, Appl. Nanosci. **11**, 1075 (2021).
[8]E. Blundo, E. Cappelluti, M. Felici, G. Pettinari, and A. Polimeni, Appl. Phys. Rev. **8**, 021318 (2021).
[9]C. Si, Z. Sun, and F. Liu, Nanoscale **8**, 3207 (2016).
[10]G. G. Naumis, S. Barraza-Lopez, M. Oliva-Leyva, and H. Terrones, Rep. Prog. Phys. **80**, 096501 (2017).
[11]S. Deng, A. V. Sumant, and V. Berry, Nano Today **22**, 14 (2018).
[12]Y. Sun and K. Liu, J. Appl. Phys. **125**, 082402 (2019).
[13]Z. Dai, L. Liu, and Z. Zhang, Adv. Mater. **31**, 1805417 (2019).
[14]T. Huang, W. Wei, X. Chen, and N. Dai, Ann. Phys. **531**, 1800465 (2019).
[15]G. Tsutsui, S. Mochizuki, N. Loubet, S. W. Bedell, and D. K. Sadana, AIP Adv. **9**, 030701 (2019).
[16]Z. Peng, X. Chen, Y. Fan, D. J. Srolovitz, and D. Lei, Light Sci. Appl. **9**, 190 (2020).
[17]C. Lee, X. Wei, J. W. Kysar, and J. Hone, Science **321**, 385 (2008).
[18]A. Castellanos-Gomez, M. Poot, G. A. Steele, H. S. J. van der Zant, N. Agraït, and G. Rubio-Bollinger, Adv. Mater. **24**, 772 (2012).
[19]A. Castellanos-Gomez, M. Poot, G. A. Steele, H. S. van der Zant, N. Agraït, and G. Rubio-Bollinger, Nanoscale Res. Lett. **7**, 233 (2012).
[20]H. J. Conley, B. Wang, J. I. Ziegler, R. F. Haglund, S. T. Pantelides, and K. I. Bolotin, Nano Lett. **13**, 3626 (2013).
[21]K. He, C. Poole, K. F. Mak, and J. Shan, Nano Lett. **13**, 2931 (2013).
[22]W. Ma, P. Alonso-gonzález, S. Li, A. Y. Nikitin, J. Yuan, J. Martín-Sánchez, J. Taboada-Gutiérrez, I. Amenabar, P. Li, S. Vélez, C. Tollan, Z. Dai, Y. Zhang, S. Sriram, K. Kalantar-Zadeh, S. T. Lee, R. Hillenbrand, and Q. Bao, Nature **562**, 557 (2018).
[23]F. Xia, H. Wang, and Y. Jia, Nat. Commun. **5**, 4458 (2014).
[24]Y. Wang, S. Yao, P. Liao, S. Jin, Q. Wang, M. J. Kim, G. J. Cheng, and W. Wu, Adv. Mater. **32**, 2002342 (2020).
[25]Z. Shu, Q. Peng, P. Huang, Z. Xu, A. A. Suleiman, X. Zhang, X. Bai, X. Zhou, and T. Zhai, Matter **2**, 977 (2020).
[26]L. Li, W. Han, L. Pi, P. Niu, J. Han, C. Wang, Y. Bando, and T. Zhai, InfoMat **1**, 54 (2019).
[27]X.-Z. Li, J. Xia, L. Wang, Y.-Y. Gu, H.-Q. Cheng, and X.-M. Meng, Nanoscale **9**, 14558 (2017).
[28]H. Song, T. Li, J. Zhang, Y. Zhou, J. Luo, C. Chen, B. Yang, C. Ge, Y. Wu, and J. Tang, Adv. Mater. **29**, 1700441 (2017).
[29]J. He, D. He, Y. Wang, Q. Cui, M. Z. Bellus, H.-Y. Chiu, and H. Zhao, ACS Nano **9**, 6436 (2015).
[30]J. O. Island, A. J. Molina-Mendoza, M. Barawi, R. Biele, E. Flores, J. M. Clamagirand, J. R. Ares, C. Sánchez, H. S. J. van der Zant, R. D'Agosta, I. J. Ferrer, A. Castellanos-Gomez, R. D'Agosta, I. J. Ferrer, and A. Castellanos-Gomez, 2D Mater. **4**, 022003 (2017).
[31]H. Li, G. Sanchez-Santolino, S. Puebla, R. Frisenda, A. M. Al-Enizi, A. Nafady, R. D'Agosta, and A. Castellanos-Gomez, Adv. Mater. **34**, 2103571 (2022).
[32]W. Luo, A. D. Oyedele, Y. Gu, T. Li, X. Wang, A. V. Haglund, D. Mandrus, A. A. Puretzky, K. Xiao, L. Liang, and X. Ling, Adv. Funct. Mater. **30**, 2003215 (2020).
[33]G. Zhang, S. Huang, A. Chaves, C. Song, V. O. Özçelik, T. Low, and H. Yan, Nat. Commun. **8**, 14071 (2017).
[34]Y. Li, Z. Hu, S. Lin, S. K. Lai, W. Ji, and S. P. Lau, Adv. Funct. Mater. **27**, 1600986 (2017).
[35]W. Zhu, L. Liang, R. H. Roberts, J.-F. Lin, and D. Akinwande, ACS Nano **12**, 12512 (2018).
[36]S. Tongay, H. Sahin, C. Ko, A. Luce, W. Fan, K. Liu, J. Zhou, Y.-S. Huang, C.-H. Ho, J. Yan, D. F. Ogletree, S. Aloni, J. Ji, S. Li, J. Li, F. M. Peeters, and J. Wu, Nat. Commun. **5**, 3252 (2014).
[37]E. Liu, Y. Fu, Y. Wang, Y. Feng, H. Liu, X. Wan, W. Zhou, B. Wang, L. Shao, C.-H. Ho, Y.-S. Huang, Z. Cao, L. Wang, A. Li, J. Zeng, F. Song, X. Wang, Y. Shi, H. Yuan, H. Y. Hwang, Y. Cui, F. Miao, and D. Xing, Nat. Commun. **6**, 6991 (2015).
[38]Y.-C. Lin, H.-P. Komsa, C.-H. Yeh, T. Björkman, Z.-Y. Liang, C.-H. Ho, Y.-S. Huang, P.-W. Chiu, A. V. Krasheninnikov, and K. Suenaga, ACS Nano **9**, 11249 (2015).
[39]D. A. Chenet, O. B. Aslan, P. Y. Huang, C. Fan, A. M. van der Zande, T. F. Heinz, and J. C. Hone, Nano Lett. **15**, 5667 (2015).
[40]O. B. Aslan, D. A. Chenet, A. M. van der Zande, J. C. Hone, and T. F. Heinz, ACS Photonics **3**, 96 (2016).
[41]F. Liu, S. Zheng, X. He, A. Chaturvedi, J. He, W. L. Chow, T. R. Mion, X. Wang, J. Zhou, and Q. Fu, Adv. Funct. Mater. **26**, 8 (2015).
[42]H. Yang, H. Jussila, A. Autere, H.-P. Komsa, G. Ye, X. Chen, T. Hasan, and Z. Sun, ACS Photonics **4**, 3023 (2017).
[43]A. Castellanos-Gomez, M. Buscema, R. Molenaar, V. Singh, L. Janssen, H. S. J. van der Zant, and G. A. Steele, 2D Mater. **1**, 011002 (2014).
[44]R. Frisenda, E. Navarro-Moratalla, P. Gant, D. Pérez De Lara, P. Jarillo-Herrero, R. V. Gorbachev, and A. Castellanos-Gomez, Chem. Soc. Rev. **47**, 53 (2018).
[45]Q. Zhao, T. Wang, Y. K. Ryu, R. Frisenda, and A. Castellanos-Gomez, J. Phys. Mater. **3**, 016001 (2020).

[46]Y. Feng, W. Zhou, Y. Wang, J. Zhou, E. Liu, Y. Fu, Z. Ni, X. Wu, H. Yuan, F. Miao, B. Wang, X. Wan, and D. Xing, Phys. Rev. B **92**, 054110 (2015).
[47]N. R. Pradhan, A. McCreary, D. Rhodes, Z. Lu, S. Feng, E. Manousakis, D. Smirnov, R. Namburu, M. Dubey, A. R. Hight Walker, H. Terrones, M. Terrones, V. Dobrosavljevic, and L. Balicas, Nano Lett. **15**, 8377 (2015).
[48]S. Yu, H. Zhu, K. Eshun, C. Shi, M. Zeng, and Q. Li, Appl. Phys. Lett. **108**, 191901 (2016).
[49]R. Frisenda, Y. Niu, P. Gant, A. J. Molina-Mendoza, R. Schmidt, R. Bratschitsch, J. Liu, L. Fu, D. Dumcenco, A. Kis, D. P. De Lara, and A. Castellanos-Gomez, J. Phys. D: Appl. Phys. **50**, 074002 (2017).